Monitoring of Railway Deformations using Distributed Fiber Optic Sensors

F. Klug, S. Lackner, W. Lienhart
Institute of Engineering Geodesy and Measurement Systems (IGMS),
Graz University of Technology, Steyrergasse 30/II, Graz, Styria, Austria,

Abstract. Natural phenomena like earthquakes, landslides, avalanches or mud flows can cause severe damages of railway tracks. Today's monitoring concepts either focus on a permanent monitoring of known problematic sites or an epoch-wise measurement of the railway track with special measurement cars.

In this paper we present a new approach for continuous monitoring of railway tracks over long distances. The new concept is based on optical fibers which are attached to the rail and depict occurring strain. The strain development can be measured with distributed fiber optic measurement instruments. Measurement ranges of several tenths of kilometers are possible with state-of-the-art equipment based on Brillouin backscattering.

We report about the measurement concept and demonstrate how vertical and horizontal deformations can be derived from strain measurements. We also focus on technologic aspects such as precision, calibration and temperature compensation. Finally, the feasibility is shown in two field experiments. In the first experiment, an existing railway track was equipped with the fiber optic sensing cable and deformed. These deformations were depicted with the distributed fiber optic sensing system and compared to point-wise deformation measurements of a total station. In the second experiment we demonstrate that also small deformations caused for instance by the dead weight of a locomotive or passenger wagon can be measured reliably.

As a conclusion distributed fiber optic sensors complement existing railway monitoring solutions and are well suited for the identification of problematic sites which have to be monitored additionally with total stations or GNSS sensors.

Keywords. fiber optic sensors, distributed sensing, railway deformations, deformation monitoring

1 Introduction

Within the last decade railway connections have become of major importance in the European transportation network. Outages due to rail track deformations, rail cracks or rail blockages are costly and can be hazardous if detected too late, see Figure 1.

Fig. 1 Derailment of passenger car in the vicinity of Tiefencastel, Switzerland (KEYSTONE/Arno Balzarini)

A distributed sensing system can reduce the maintenance costs and increase the reliability by early detections of critical events. One promising technology for the automated and continuous monitoring is distributed fiber optic sensing (FOS) based on Brillouin backscattering. Already today, several tenths of kilometers of fiber optic cables can be monitored with a single instrument.

2 Principle of Brillouin Measurements

Brillouin scattering is caused by acoustic-optical interaction when light is travelling in an optical fiber (e.g. Hayashi et al., 2014; Nöther, 2010). This interaction can be stimulated by a high power laser in case of Brillouin Optical Time Domain Reflectometry (BOTDR) or by using a loop configuration with a continuous pump laser and a pulse laser which emits light pulses (BOTDA,

Brillouin Optical Time Domain Analyzer) or amplitude modulated waves (BOFDA, Brillouin Optical Frequency Domain Analyzer), see Figure 2.
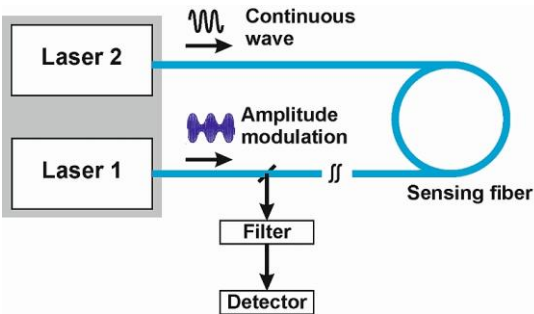
Fig. 2 Overview of BOFDA loop configuration

With this configuration a measurement range of several tenths of kilometers and a spatial resolution of better than 1m are possible. The sensing principle is based on the fact that the Brillouin frequency shift changes linearly with temperature and strain (Zeni et al., 2015, Kurashima et al., 1990). The measurement unit records the frequency shift as well as the position along the fiber.
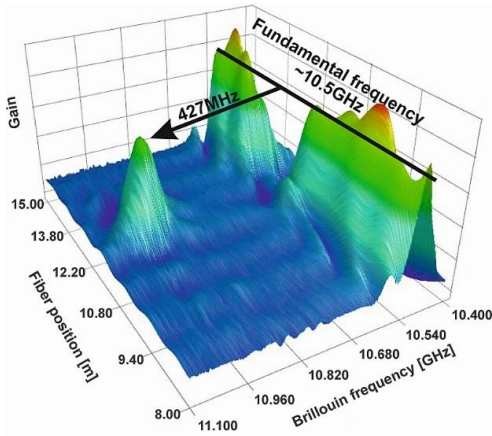
Fig. 3 3D-spectrum of a BOFDA measurement

Figure 3 shows a characteristic result of a Brillouin measurement along 7m of glass fiber. The center frequency of the unstrained fiber is located at 10.5GHz. Strain was applied at one fiber position (~13m) which causes a significant shift of the Brillouin frequency of 427MHz. This frequency shift can be converted into strain or temperature values if the conversion coefficients are known. Since the frequency shift depends on strain and temperature, appropriate temperature compensation is needed for accurate strain measurements. One

possibility is the parallel installation of a strained and loose fiber. The measurement of the pre-strained fiber is sensitive to strain and temperature whereas the loose fiber only reacts to temperature changes. As will be shown in section 4 of this paper, both measurement values can be used to derive temperature compensated strain.

3 Measurement Concept

Reliable monitoring of railway tracks is only possible with a rigid connection between sensing fiber and rail. The sensing fiber can either be glued to a rail (Zeni et al., 2015) or connected with clamps at specific points. We followed the second approach and designed a special sensing cable clamp which consists of a base and a cover plate (Figure 4). The cover plate can be used for laboratory and field installations, the base plate is adaptable to different track sizes and to laboratory setups.
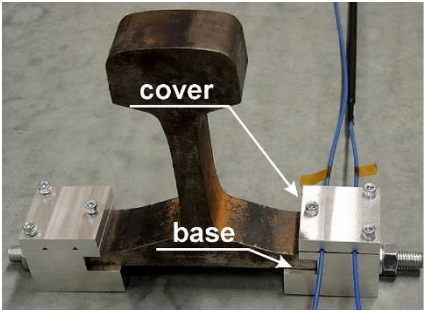
Fig. 4 Sensing cable clamp

The clamps are placed in between the railway sleepers (Figure 5). During installation the strain sensing fiber is pre-strained to enable the measurement of elongation (positive strain) and shortening (negative strain). A loose fiber is placed parallel to the strain fiber for temperature compensation. If bending should be derived the setup has to be implemented on both sides of the rail. All fibers form one loop and the two ends are connected to the instrument.
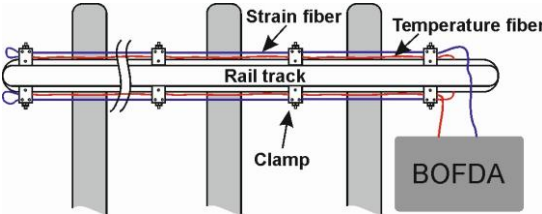
Fig. 5 Monitoring layout

4 Laboratory Investigations

Approximate values for strain and temperature coefficients of sensor cables are typically given by the manufacturer. For achieving highest accuracy we calibrated the selected BRUsens V1 cable (Brugg Cables, 2013) on our unique fiber optic calibration facility (Presl, 2009). For the laboratory and field installations we used a fTB2505 instrument from Fibris Terre Systems (Fibris Terre Systems, 2015).

4.1 Temperature Calibration

Every fiber optic strain sensing cable is temperature sensitive. This relation is usually expressed by a linear temperature coefficient k_T:

$$k_T = \frac{\Delta \nu_T}{\Delta T} \qquad (1)$$

In order to determine the temperature coefficient, a sample of the chosen sensing cable was placed into a climate chamber and exposed to specific temperature cycles. Using these data the temperature coefficients were determined by least squares adjustment. Our calibrated temperature coefficient differs about 20% from the approximate value given by the manufacturer, see Table 1.

Table 1. Temperature coefficient

	Temperature coefficient k_T [MHz/K]
Brugg Cables (2013)	~4.2
IGMS	5.2

With the estimated temperature coefficient the standard deviation of the residuals could be reduced from 3.7K to 0.6K.

4.2 Strain Calibration

For the investigation of fiber optic strain sensing cables, we have developed a unique calibration facility (Presl, 2009), see Figure 6. Main components are a laser interferometer that is used as the reference measurement system and a 300mm linear translation stage. With a modular sensor mounting system, different types of fiber optic strain sensors can be tested and calibrated (see e.g. Klug and Woschitz 2015).
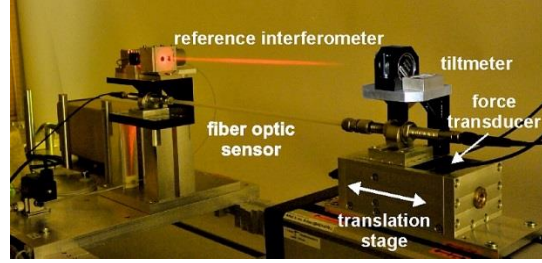
Fig. 6 IGMS FOS calibration facility

Since the reference interferometer is placed eccentrically the Abbe's comparator principle is not fulfilled. To avoid errors, two tiltmeters are used for monitoring the alignment stability of the two anchor platforms. For fatigue and load testing, a force transducer (max. 2kN) can be used which is mounted inside a special housing on the translation stage.

The controlling software permits different settings and calibration profiles. The whole system provides fully automatic operation and data acquisition. The calibration facility is set up in our temperature and humidity controlled laboratory on a rail system mounted at a stable concrete bench with a length of 30m. For quality assurance the laboratory temperature is monitored by temperature sensors along the concrete bench and usually remains stable within 0.1K during the calibration period.

The accuracy of the calibration facility depends on the maximum strain and the sensor length. For example, for a 5m long strain transducer which is strained for 30 000µm/m, the expanded standard uncertainty of the reference system (determined in accordance to GUM, JCGM, 2008) is about $U_{\Delta L} = \pm 2.5 \mu m$ (k = 2) for the measured length changes ΔL. This corresponds to an expanded standard uncertainty in strain of about $U_\varepsilon = \pm 0.5 \mu m/m$.

The result of a strain calibration is the linear strain coefficient k_ε which is defined as

$$k_\varepsilon = \frac{\Delta \nu_\varepsilon}{\Delta \varepsilon} \qquad (2)$$

We performed several calibration runs with the BRUsens V1 cable. In a typical strain calibration, the sensor was elongated four times from 1 to 6mm in steps of 0.5mm (Figure 7, top). By using the reference interferometric data and the Brillouin frequencies, the strain coefficient was estimated by least squares adjustment, see Table 2.
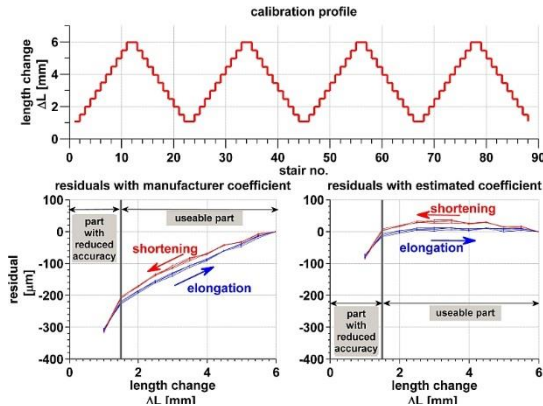
Fig. 7 Comparison of residuals using approximate (bottom left) and estimated strain coefficient (bottom right)

Table 2. Strain coefficient

	Strain coefficient k_ε [MHz/%]
Brugg Cables (2013)	~450
IGMS	476

Figure 7 bottom row shows a comparison of the residuals when using the approximate and the estimated coefficient. In both graphs it is visible that the relation between strain and Brillouin frequency shift is different at very small strain. Reliable results can therefore only be gained at strains above 0.25%. This section has been excluded from the further analysis. When using the approximate coefficient from the manufacturer the residuals show a linear trend of about 47µm per mm of length change. This represents a systematic error of approx. 5%. The results of the individual calibration cycles are reproducible and fit well, however a hysteresis between shortening and elongation occurs in all calibration runs. This hysteresis is the main cause for the reaming residuals which are within ±30 µm.

For the sensor calibration the temperature and strain dependency have been investigated separately. The strain calibration was performed at stable temperature in the air conditioned laboratory and the temperature calibration was made in the climate chamber with no strain applied. In field installation both effects occur simultaneously. For calculating temperature compensated strain the following equation has to be applied (ASTM, 2014)

$$\Delta\varepsilon = \frac{\Delta v_\varepsilon}{k_\varepsilon} - \frac{k_T^* * \dfrac{\Delta v_T}{k_T}}{k_\varepsilon} \qquad (3)$$

The raw measurement values are the Brillouin frequency shifts of the strain and temperature cable Δv_ε and Δv_T. The linear coefficients k_ε and k_T are determined in the laboratory calibration. The coefficient k_T^* represents the thermal optical coefficient for the used bare fiber. This coefficient is defined with k_T^*=1.1MHz/K by the cable manufacturer.

4.3 Detectable Deformation

A fiber optic sensor is highly sensitive in the longitudinal axis. As a consequence lateral rail deformations act in the non-sensitive axis of the sensing cable. Therefore, we built a test setup with two fixed anchoring points and one moveable point, see Figure 8. The central anchoring point is moveable in lateral direction with a linear translation stage. The lateral deformation is recorded independently by a triangulation sensor.
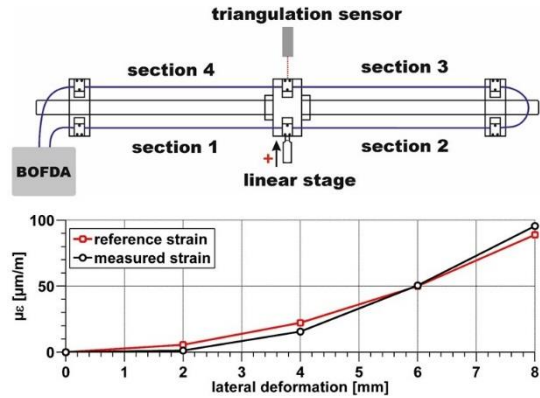
Fig. 8 Test setup and results for section 4

Figure 8 shows the calculated strain using the triangulation sensor data and the fiber optic measurements of section 4. It is clearly visible that the lateral deformations can be detected with the deployed BOFDA measurement system.

4.4 Sensor Tension Tests

With respect to possible rail cracks we tested the maximum tension of the installed sensing cable. The manufacturer (Brugg Cables, 2013) of the sensing cable specifies a maximum tension of 1% (10 000µm/m). Under harsh ambient conditions a rail crack can have a width of a few centimeters. Dependent on the anchoring distance, this results in a tension of several percent.

4

To test the load limits for short term and long term measurements of the used sensing cable we performed two experiments. The first experiment focused on the absolute load limit for short term conditions. We used our calibration facility in this experiment to continuously increase the tension of the sensing cable until the fiber broke, see Figure 9.
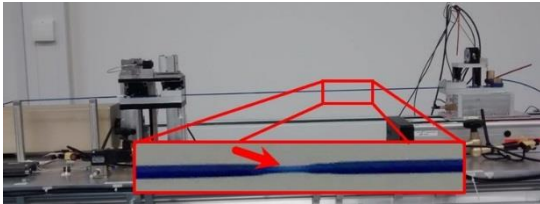
Fig. 9 Fiber failure test on the calibration facility

The breaking level of the investigated sensing cable was between 8% and 9%. This corresponds to a length change of about 50mm at the anchoring distance of 0.6m.

To investigate the long term stability at high strain we permanently mounted a sensing cable with an initial pre-strain of ~3.5% at a stable position in the laboratory, see Figure 10.
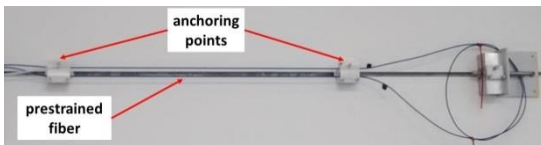
Fig. 10 Setup of the long term high strain test

Measurements over a period of 3 months indicate that the initial pre-strain is decreasing over time. Figure 11 shows three measurements of this experiment. In the first measurement the pre-strained area is clearly detectable.
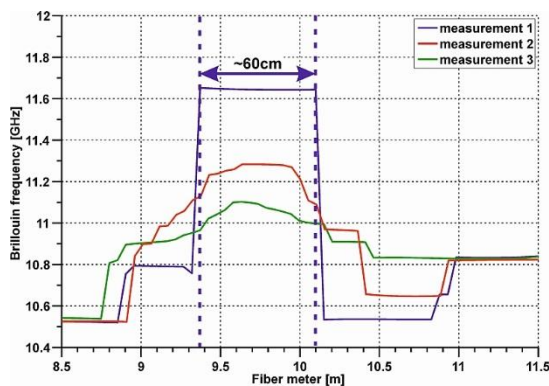
Fig. 11 Long term high strain test

Gradually the strain decreases dramatically and spreads out in cable sections outside of the anchoring points. We suppose that this effect is a result of the structure of the used soft sensing cable. From these experiments it can be concluded that the sensing cable withstands strains much higher than the specified 1% but the measurements will be biased with respect to spatial allocation and maximum strain value.

5 Field Tests

We also performed two field experiments to simulate distinct events. One test focused on large vertical loads and the second on lateral rail deformations which can be caused by natural events, like landslides, mudflows or underwashing. The goal was to verify if such events can be detected with a distributed fiber optic system. To validate the results, independent geodetic measurements were performed.

Final goal of structural monitoring is to separate deformations caused by regular behavior of the structure from deformations caused by adverse events. To determine strain changes $\Delta\varepsilon_{event}$ caused by events like landslides the regular strain changes of the rail due to temperature changes $\Delta\varepsilon_{rail,T}$ have to be subtracted from the measured strain changes $\Delta\varepsilon$ of equation (3). This relation is expressed in equation (5) where the temperature induced material elongation of the rail is taking into account.

$$\Delta\varepsilon_{event} = \Delta\varepsilon - \Delta\varepsilon_{rail,T} \qquad (5)$$

$\Delta\varepsilon_{rail,T}$ depends on various factors, like the thermal expansion of the rail material or the geometry of the track (straight section, curved section).

5.1 Geodetic Measurements

To verify the fiber optic measurements, geodetic measurements were carried out in the two field tests using a Leica TS15 total station. For both tests a local reference network was established in advance to compare the total station observations of all load experiments in a common coordinate frame. The x-axis of the coordinate system was aligned to the rail track direction. Therefore, coordinate changes in x-direction represent lateral rail displacements. Regular temperature and pressure measurements

5

were used to correct the electronic distance measurements.

In the first field test (see section 5.2) the positions of the clamps, mounted on the rail track were determined using a Leica mini prism GMP111, that was placed into a special drilling hole of the rail clamp, see Figure 12 (left). In the second field test (see section 5.3) reflective tapes were mounted on the clamps to enable manual contact-less measurements of the height changes during the load tests, see Figure 12 (right).
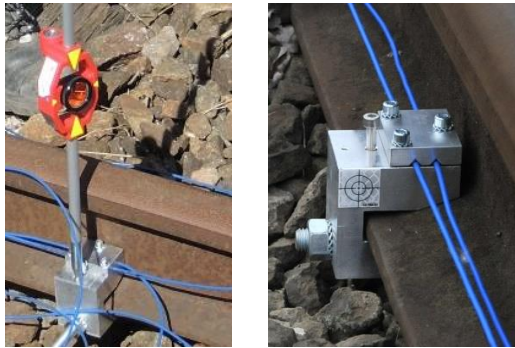
Fig. 12 Measurement position on clamp using Leica mini prism GMP111 (left) or a reflective tape (right)

5.2 Natural Events

The first field installation focused on natural events where the rail track is locally deformed. Such an event can be caused by a landslide, an avalanche, a mudflow or a rock slide. All these events represent a high risk to people and the rail infrastructure. For these tests one rail was equipped on both sides with a distributed fiber optic measurement cable. To simulate a natural event we deformed the rail track laterally with a winch as is shown in Figure 13.

Fig. 13 Fiber optic setup and lateral deformation using a winch for simulating natural events

Geodetic and fiber optic deformation measurements were carried out after each deformation step. Figure 14 displays the results of the geodetic measurements for three different deformation steps. It can be seen that the rail was locally displaced for about 30mm in lateral direction.
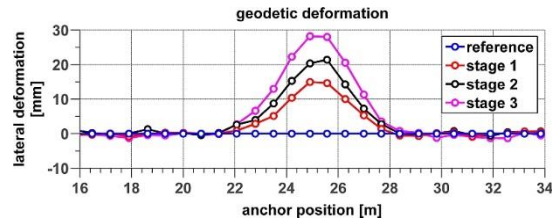
Fig. 14 Lateral displacements of the rail measured with a total station

It is important to note that geodetic measurements result in coordinate changes within a stable reference frame. On the contrary fiber optic systems measure relative changes of the monitored object. Hence, fiber optic measurements are insensitive to rigid body motions but highly sensitive to longitudinal strain or bending. A local lateral displacements results in a sequence of positive and negative strain on both sides of the rail as indicated in Figure 15.
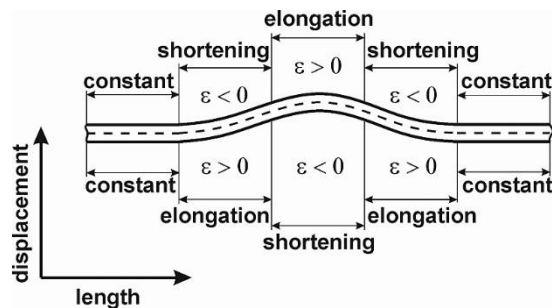
Fig. 15 Length changes of both sides of a rail due to local lateral displacements

Figure 16 shows the results of the fiber optic measurements. The expected pattern of shortening and elongation is clearly visible. Hence, it can be concluded that lateral rail displacements can be depicted with distributed fiber optic strain measurements.
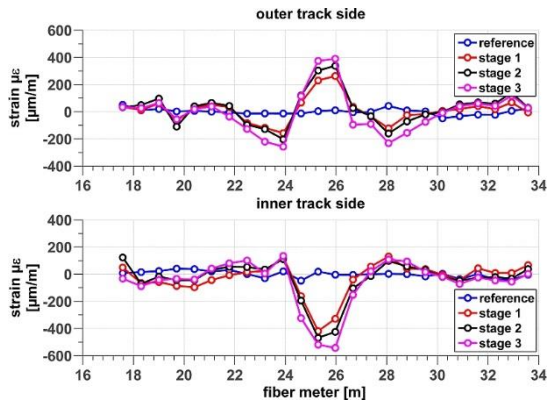
Fig. 16 Measured strain changes on the outer and inner track side

5.3 Load Tests

The second field installation focused on vertical deformations of a rail track. Therefore, different loads - in our case a locomotive and a passenger wagon were placed on the instrumented rail, see Figure 17 and Table 3.

Fig. 17 Load test with a locomotive (left) and a passenger wagon (right)

Table 3. Data of applied load

	Overall length [m]	Weight [t]
Locomotive	19.28	80
Passenger wagon	26.40	46

The resulting length change of the fiber optic sensing cable was measured with the distributed fiber optic system. Figure 18 shows the results of this experiment. Although heavier than the passenger wagon, the locomotive caused only small vertical deformations of less than 2mm. The impact of the four axes can be identified in the geodetic measurements but is hardly visible in the fiber optic measurements. In the second part of the experiment the locomotive was replaced by the passenger

wagon. This wagon was positioned so that one ring was located at the same position as the ring unit of the locomotive. The second ring unit was at a different position due to the longer length of the wagon. At this position vertical deformations of more than 5mm occurred. It is assumed that the reasons of these large deformations are not well compacted foundations in this area. The fiber optic strain measurements also yield high strain values in this section. This demonstrates that also vertical rail deformations which may be caused by underwashing can be detected with distributed fiber optic measurements.
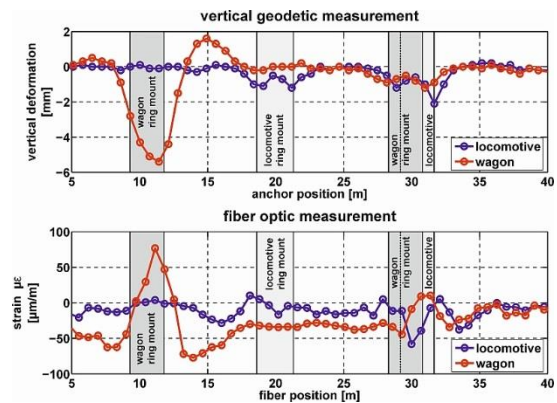
Fig. 18 Vertical displacements (top) and measured strain (bottom) due to locomotive load (blue) and passenger wagon (red)

6 Conclusion

Undetected rail track deformations or rail cracks are a potential risk for passengers, rail freight and the railway infrastructure. In this paper we demonstrated a new approach to monitor rail tracks over long distances by using distributed fiber optic measurements.

The advantage of the fiber optic concept is that distances of several tenths of kilometers can be monitored with a single instrument. We demonstrated that local strain measurements are suitable to detect local track displacements of a few millimeters.

In case of rail cracks the sensing cable has to withstand high strain values. With the selected sensing cable and the used anchor spacing the sensing system can cope with cracks of with lengths of several centimeters.

Critical aspects for achieving accurate results are a rigid connection of the sensing cable to the rail,

correct conversion coefficients and temperature correction of Brillouin shift values. We therefore developed a special rail clamp, performed temperature and strain calibration of the sensing cable and attached pre-strained and loose cables.

Acknowledgements

References

ASTM (2014). ASTM F3079-14, Standard Practice for Use of Distributed Optical Fiber Sensing Systems for Monitoring the Impact of Ground Movements During Tunnel and Utility Construction on Existing Underground Utilities, ASTM International, West Conshohocken, PA, 2014.

Brugg Cables (2013). BRUsens Strain V1. Datasheet Rev. 04.

Fibris Terre Systems GmbH (2015). fTB 2505 Fiber-optic sensing system for distributed strain and temperature monitoring. Datasheet.

Hayashi N., Mizuno Y. and Nakamura K. (2014). Alternative implementation of simplified Brillouin optical correlation-domain reflectometry. In: IEEE, DOI: 10.1109/JPHOT.2014.

JCGM (2008). Evaluation of measurement data- Guide to the expression of uncertainty in measurement. In: JCGM Publication 100, www.bipm.org, 134 p.

Klug F. and Woschitz W. (2015). Test and calibration of 20 FBG based strain transducers. In Proc. 7th Int. Conf. on Structural Health Monitoring of Intelligent Infrastructure - SHMII, Turin, Italy, 11 p.

Kurashima T., Horiguchi T. and Tateda M. (1990). Thermal Effects of Brillouin Gain Spectra in Single-Mode Fibers. In: IEEE Photonics Technology Letters, Vol. 2, pp. 718-720.

Nöther N. (2010). Distributed Fiber Sensors in River Embarkments. Advancing and Implementing the Brillouin Optical Frequency Domain Analysis. In: BAM-Dissertationsreihe, Volume 64.